Progress In Electromagnetics Research, Vol. 157, 121–131, 2016

The Factorization Method for Virtual Experiments Based Quantitative Inverse Scattering

Lorenzo Crocco[1, *], Loreto Di Donato[2], Ilaria Catapano[1], and Tommaso Isernia[1, 3]

Abstract—The concept of virtual experiments is based on the idea of solving the inverse scattering problem by processing a suitable recombination of the available data, instead of those arising from the measurements. By properly designing such experiments (and without additional measurements), it is possible to enforce some peculiar field's or contrast source's properties, which can be helpful to perform the inversion in a more simple and reliable way. In this paper, we show that the factorization method can be used as a tool to design the virtual experiments. In doing so, we also provide, for the first time, an insight into its physical meaning. As an example, we exploit the virtual experiments designed via FM as the backbone of a linearized inversion approach for quantitative imaging of non-weak targets.

1. INTRODUCTION

Inverse scattering problems consist in determining morphologic and constitutive features of unknown targets from the field they scatter [1]. Basically, these problems can be grouped into two classes. In the *inverse obstacle* problem, the aim is to retrieve the location and the shape of objects whose constitutive features may be either known or unknown. In the *inverse medium* problem the complete characterization of the targets is pursued. In both cases, one has to solve a non-linear and ill-posed problem.

Qualitative methods [2] provide an effective way to tackle the inverse obstacle problem, as they can reconstruct the shape of dielectric or metallic not convex and/or not connected objects by relying on the behavior of an *indicator* function. This latter is obtained as the solution of an auxiliary linear and ill-posed inverse problem, so that qualitative methods are typically easy to implement and computationally efficient. Notably, such a simplification is not achieved through approximations, but it is based on the explicit restriction of the scope of the inversion task. As a matter of fact, qualitative methods cannot provide any information on the nature of the targets. Several qualitative methods have been developed in the literature [2, 3] and the most popular are the linear sampling method (LSM) [4] and the factorization method (FM) [5].

In a recent series of papers [6–11], it has been shown that it is possible to take advantage of the information achieved from the LSM not only to estimate the unknown target's support, but also to introduce new quantitative inversion methods. These latter are capable of retrieving the electromagnetic parameters of the unknown targets using linear approximations that hold true for non-weak scatterers [6, 7], localized non-linear approximations [8] or new regularization schemes [9, 10].

The unifying idea underlying these methods is the simple observation that a combination (i.e., a linear superposition) of the experiments performed to produce the problem's data can give raise to a new, *virtual*, experiment, without requiring additional measurements. By properly choosing the

Received 28 July 2016, Accepted 29 October 2016, Scheduled 15 November 2016

* Corresponding author: Lorenzo Crocco (crocco.l@irea.cnr.it).

[1] Institute for Electromagnetic Sensing of the Environment, National Research Council of Italy (IREA-CNR), I-80124, Napoli, Italy.

[2] Dipartimento di Ingegneria Elettrica, Elettronica e Informatica (DIEEI), University of Catania, I-95126, Catania, Italy.

[3] Dipartimento di Ingegneria dell'Informazione, delle Infrastrutture e dell'Energia Sostenibile (DIIES), Mediterranea University of Reggio Calabria, I-89060, Reggio Calabria, Italy.

combination coefficients, peculiar properties can be enforced on the *virtual* fields and contrast sources. Accordingly, the imaging problem can be conveniently tackled by relying on such properties.

With reference to the 2D scalar inverse scattering problem (TM polarization), in this paper, we show that it is possible to use the FM to design the virtual experiments (VE). To this end, we derive an original rewriting of the FM equation that, for the first time, discloses the physical meaning of FM. Notably, this new way to design VE stands on a sound theoretical basis, since FM allows to overcome the well known issues arising in LSM [5, 12].

It is worth noting that the VE provide a general framework to tackle inverse scattering, as they can be paired with any inversion method, by using the virtual fields and taking into account the specific properties enforced by the VE. For instance, the VE can be used within the contrast source inversion method [9] or within the distorted Born method [11]. On the other hand, one of the most interesting aspects of VE is the capability of quantitatively imaging non-weak targets via linear inversion [6, 7]. For this reason, as an example of how using FM-designed VE for imaging purposes, we adopt them within the linearized inversion method introduced in [6] to process some experimental data belonging to the Fresnel database [13, 14] typically used to benchmark inversion methods for non-weak targets.

The paper is organized as follows. In Section 2, we formulate the problem and recall the VE framework. In Section 3, we recall the FM basics, while in Section 4 we provide a rewriting of the FM equation which allows to understand how to use it to design a set of VE. In Section 5, we introduce the new FM based method for quantitative imaging and discuss its implementation. Section 6 is concerned with the assessment of the presented results. Conclusions and possible extensions follow.

2. FORMULATION OF THE PROBLEM AND VIRTUAL SCATTERING EXPERIMENTS

Let Σ denote the (possibly not connected) support of a dielectric scatterer of relative complex permittivity $\tilde{\varepsilon}_x(\underline{r})$, $\underline{r} = (x, y)$, whose cross-section is invariant along the z-axis. The targets are enclosed within the imaging domain Ω, embedded in a homogeneous, possibly lossy, medium of complex permittivity $\tilde{\varepsilon}_b$. The magnetic permeability is everywhere that of vacuum μ_0.

The targets are probed through a set of sources lying on a curve Γ located in the far zone of the scatterers, i.e., at a distance $R > 2d^2/\lambda$, d being the size of Ω and λ the wavelength in the host medium. Assuming unitary excitations sources, the resulting incident fields in $\underline{r} \in \Omega$ can be approximated with unitary plane waves as:

$$E_{inc}(\underline{r}, \theta) = e^{-jk\hat{\theta}\cdot\underline{r}}, \tag{1}$$

where a time factor $\exp(j\omega t)$ has been assumed and omitted, and k is the background wave-number and $\hat{\theta}$ the unit vector denoting the angular position θ of the source.

For a generic incident field, the scattering phenomenon can be cast via the pair of integral equations:

$$E_s(\underline{R}, \theta) = \int_\Omega G(\underline{R}, \underline{r}')E_t(\underline{r}', \theta)\chi(\underline{r}')d\underline{r}', \tag{2}$$

$$E_t(\underline{r}, \theta) = E_{inc}(\underline{r}, \theta) + \int_\Omega G(\underline{r}, \underline{r}')E_t(\underline{r}', \theta)\chi(\underline{r}')d\underline{r}', \tag{3}$$

where $\underline{R} = (R, \varphi) \in \Gamma$, E_s denotes the scattered field, E_t the total field, G the free space Green's function and χ the contrast function:

$$\chi(\underline{r}) = \frac{\tilde{\varepsilon}_x(\underline{r})}{\tilde{\varepsilon}_b} - 1. \tag{4}$$

The (nonlinear and ill-posed) inverse scattering problem consists of retrieving the contrast χ from the knowledge of E_s on Γ and E_{inc} in Ω.

2.1. The Virtual Experiments

From Eqs. (2), (3), one can observe that the relationship between the scattered field and the incident field is linear (for a fixed contrast function). This suggests that if the sources are weighted by some

excitation function $w(\theta)$, the resulting incident field:

$$\Psi_{inc}(\underline{r}) = \int_{\Gamma} w(\theta) e^{-jk\hat{\theta}\cdot\underline{r}} d\theta \tag{5}$$

will induce a scattered field given by:

$$\Psi_s(\underline{R}) = \int_{\Gamma} w(\theta) E_s(\underline{R}, \theta) d\theta. \tag{6}$$

To obtain the field in Eq. (6), one does not need additional measurements, hence the scattering experiment identified by Ψ_{inc} can be seen as a *virtual* experiment. Notably, by properly assigning weighting function $w(\theta)$, virtual experiments can be designed in such a way to enforce some peculiar properties useful or helpful to tackle the inverse scattering problem.

In [6–11], the design of the VE exploits the integral equation at the core of LSM. To recall this procedure, let us introduce the far-field operator [1]:

$$\mathcal{F} : i(\theta) \in L^2(\Gamma) \rightarrow \int_{\Gamma} E_{\infty}(\varphi, \theta) i(\theta) ds(\theta) \in L^2(\Gamma), \tag{7}$$

wherein $E_{\infty}(\varphi, \theta)$ is the so-called far-field pattern pertaining to the target, which is related to the asymptotic behavior ($R \rightarrow \infty$) of the scattered field as:

$$E_s(\underline{R}, \theta) = \frac{e^{-jkR}}{\sqrt{R}} E_{\infty}(\varphi, \theta) + O\left(R^{-3/2}\right). \tag{8}$$

In view of Eqs. (5), (6) and (8), the far-field operator $\mathcal{F}$ has a straightforward physical interpretation, as the operator that provides the scattered far-field pattern due to the excitation distribution $i(\theta)$.

The integral equation that casts the LSM, the far-field equation (FFE), reads:

$$\mathcal{F}[i(\theta, \underline{r}_p)] = \Psi_{\infty}(\underline{r}_p, \varphi), \tag{9}$$

wherein Ψ_{∞} denotes the far-field pattern of an elementary source positioned in $\underline{r}_p \in \Omega$. Note the unknown function i now depends on both θ and $\underline{r}_p$, since the solution of Eq. (9) changes with the position of the elementary source. It is easy to understand that the FFE in Eq. (9) can be used to design a virtual experiment in which the virtual scattered field corresponds (on Γ) to the field Ψ_{∞} radiated by a point source located in $\underline{r}_p$. Such a virtual experiment will be driven by the excitation function $i(\theta, \underline{r}_p)$ obtained from the design Eq. (9). Notably, by changing the *pivot* point $\underline{r}_p$, different experiments can be designed. In this respect, a convenient way to choose the *pivot* points is to pick them among the sampling points that belong to the target's support as estimated from LSM.

Finally, note that considering Ψ_{∞} is only one of the possible design goals. For instance, different fields (and therefore experiments) can be designed by replacing Ψ_{∞} with higher-order elementary fields and exploiting the "generalized" LSM equation [15].

3. THE FACTORIZATION METHOD

Similar to LSM, FM requires to sample the domain under test Ω into an arbitrary grid of points and solve in each sampling point, say $\underline{r}_p$, the linear equation:

$$\mathcal{F}_m \left[h(\theta, \underline{r}_p)\right] = \Psi_{\infty}(\underline{r}_p, \varphi), \tag{10}$$

In Eq. (10), $\mathcal{F}_m : L^2(\Gamma) \rightarrow L^2(\Gamma)$ is a linear and compact operator, whose expression depends on $\mathcal{F}$ and on the background medium's properties, as well as on the measurement configuration [5]. In the canonical case at hand, wherein the far-field operator is normal [16], this expression reads [5]

$$\mathcal{F}_m = (\mathcal{F}^{+}\mathcal{F})^{1/4}. \tag{11}$$

By denoting with $\{\mu_n, \xi_n\}$ the Singular Value Decomposition (SVD) [17] of $\mathcal{F}$, the SVD of $\mathcal{F}_m$ is expressed as $\{\mu_n, \sqrt{\xi_n}\}$ [5]. Hence, the solution of Eq. (10) is formally given as:

$$h(\theta, \underline{r}_p) = \sum_{n=0}^{\infty} \frac{1}{\sqrt{\xi_n}} \left\langle \Psi_{\infty}(\underline{r}_p, \varphi), \mu_n(\varphi) \right\rangle_{\Gamma} \mu_n(\theta), \tag{12}$$

where $\langle , \rangle$ denotes the scalar product in $L^2(\Gamma)$.

It is possible to prove that the series (12) is convergent if and only if the sampling point belongs to Σ [5]. Accordingly, the energy of h provides an *indicator* for the unknown support, which is bounded only when $\underline{r}_p \in \Sigma$, while it is unbounded elsewhere. Hence, the unknown shape is simply estimated by observing the plot of $\|h\|^2$ (usually in a logarithmic scale) over Ω [5].

As a final comment, note that since $\mathcal{F}_m$ is compact, the linear problem cast in Eq. (10) is ill-posed. Hence, it has to be solved in a regularized sense to avoid instabilities. Assuming that Tickhonov regularization is used, as typically done in practice, the regularized FM solution reads:

$$h(\theta, \underline{r}_p) = \sum_{n=0}^{\infty} \frac{\sqrt{\xi_n}}{\xi_n + \alpha} \left\langle \Psi_\infty(\underline{r}_p, \varphi), \mu_n(\varphi) \right\rangle_\Gamma \mu_n(\theta), \tag{13}$$

wherein α is the Tickhonov regularization parameter.

4. THE FACTORIZATION METHOD AND THE VIRTUAL EXPERIMENTS

4.1. A Rewriting of the FM Equation

To show how VE can be designed by exploiting FM, we first derive a different writing of Eq. (10). To this end, let us recall that the kernel of $\mathcal{F}$ is a square integrable function [1]. Hence, $\mathcal{F}$ is a Hilbert-Schmidt operator [16] and $E_\infty(\varphi, \theta)$ admits the following spectral representation, (see Eq. (9.74) in [17]):

$$E_\infty(\varphi, \theta) = \sum_{n=0}^{\infty} e_\infty^n(\varphi, \theta) = \sum_{n=0}^{\infty} \xi_n \mu_n^*(\theta) \mu_n(\varphi), \tag{14}$$

the series being convergent in the L^2 norm sense [17].

Equation (14) provides a decomposition of the far-field pattern $E_\infty(\varphi, \theta)$, in which each term e_∞^n is given by a weighted version of the far-field pattern that arises when the sources are fed with the excitation distribution $\mu_n(\theta)$. As a matter of fact, by virtue of the SVD definition, $\mathcal{F}[\mu_n(\theta)] = \xi_n \mu_n(\varphi)$, the generic element of (14) can be written as:

$$e_\infty^n(\varphi, \theta) = \xi_n \mu_n^*(\theta) \mu_n(\varphi) = \mu_n^*(\theta) \mathcal{F}\left[\mu_n\right]. \tag{15}$$

Accounting for the $\mathcal{F}_m$ expression given in Eq. (11) and the SVD properties, it follows that also $\mathcal{F}_m$ is a Hilbert-Schmidt operator [16]. As such, we can rewrite Eq. (10) as:

$$\mathcal{F}_m\left[h(\theta, \underline{r}_p)\right] = \int_\Gamma K_{FM}(\varphi, \theta) h(\theta, \underline{r}_p) ds(\theta) = \Psi_\infty(\underline{r}_p, \varphi), \tag{16}$$

where K_{FM} denotes the kernel of $\mathcal{F}_m$, which can be expressed as:

$$K_{FM}(\varphi, \theta) = \sum_{n=0}^{\infty} \sqrt{\xi_n} \mu_n^*(\theta) \mu_n(\varphi). \tag{17}$$

The above shows that the equation at the core of the FM is formally analog to the FFE in Eq. (9). However, being the kernel different, a different physical meaning is expected. To get a better insight in this point, let us exploit the SVD definition to rewrite the generic term κ_n of Eq. (17) as:

$$\kappa_n(\varphi, \theta) = \sqrt{\xi_n} \mu_n^*(\theta) \mu_n(\varphi) = \mu_n^*(\theta) \mathcal{F}\left[\frac{\mu_n(\theta)}{\sqrt{\xi_n}}\right]. \tag{18}$$

Equation (18) suggests that K_{FM} can be seen as the far-field pattern given by the superposition of the far-field patterns κ_n that arise due to the *weighted* singular excitations:

$$i_n(\theta) = \frac{\mu_n(\theta)}{\sqrt{\xi_n}} \quad n = 0, \ldots, +\infty. \tag{19}$$

Now, by taking advantage of this explicit relationship between K_{FM} and the primary currents, it is possible to rewrite in a different fashion the FM equation. In particular, one has:

$$\mathcal{F}_m[h] = \int_\Gamma K_{FM}(\varphi,\theta)h(\theta,\underline{r}_p)ds(\theta) = \int_\Gamma \sum_{n=0}^{\infty} \mu_n^*(\theta)\mathcal{F}[i_n]h(\theta,\underline{r}_p)ds(\theta) =$$
$$= \sum_{n=0}^{\infty} \int_\Gamma h(\theta,\underline{r}_p)\mu_n^*(\theta)ds(\theta)\ \mathcal{F}[i_n] = \mathcal{F}\left[\sum_{n=0}^{\infty} \left\langle h(\theta,\underline{r}_p),\mu_n(\theta)\right\rangle_\Gamma i_n(\theta)\right]. \tag{20}$$

Therefore, using Eq. (19), the FM Eq. (10) can be explicitly rewritten in terms of $\mathcal{F}$ as:

$$\mathcal{F}\left[\sum_{n=0}^{\infty} \left\langle h(\theta,\underline{r}_p),\mu_n(\theta)\right\rangle_\Gamma \frac{\mu_n(\theta)}{\sqrt{\xi_n}}\right] = \Psi_\infty(\underline{r}_p,\varphi). \tag{21}$$

The above result provides a physical interpretation of the FM. As a matter of fact, the FM equation can be now re-interpreted as the determination of an overall excitations distribution i_{FM} (function of the actual unknown h) given by:

$$i_{FM}(\theta,\underline{r}_p) = \sum_{n=0}^{\infty} \left\langle h(\theta,\underline{r}_p),\mu_n(\theta)\right\rangle_\Gamma \frac{\mu_n(\theta)}{\sqrt{\xi_n}}, \tag{22}$$

such that the corresponding far-field pattern matches the one of a point source on Γ. Notably, such a current is not the actual unknown of the equation to be solved in Eq. (10), which is instead $h(\theta)$.

As well known, considering Eq. (10) allows overcoming the theoretical drawbacks of LSM [12]. In particular, since the right-hand side of the FFE is almost never in the range of $\mathcal{F}$, the LSM indicator $\|i\|$ may diverge also for sampling points belonging to the scatterer, even in the ideal case of noiseless data. Such an unwanted outcome (which may also affect the designed VE) does not affect FM. It is interesting to notice that the above circumstance can be explained from a physical viewpoint thanks to the above given interpretation of the FM. To this end, note that, unless special cases occur, an exact fulfillment of the FFE in Eq. (9) in a generic sampling point $\underline{r}_p$ entails an impulsive behavior of the contrast source χE [18]. In case of extended targets, this requires not only that $\underline{r}_p$ belongs to the support of the scatterer, where $\chi(\underline{r}_p) \neq 0$, but also that the total field itself has an impulsive behavior. As incident fields only have a finite number of degrees of freedom [19], and the same holds true for total fields (for any fixed contrast distribution), one is not able to fulfill Eq. (9), unless *superdirective* [20] primary sources are exploited. As known, these special sources are characterized by a diverging energy, thus explaining the behavior of $\|i\|$. This issue is overcome in the FM equation (10), wherein, thanks to the presence of the factors $1/\sqrt{\xi_n}$ in Eq. (22), the indicator function $\|h\|$ may keep limited even when the energy of i_{FM} diverges. Hence, it can be concluded that by considering the function h as the problem's unknown, rather than actual excitation distribution i_{FM}, it is possible to avoid the drawbacks associated to the requirement of enforcing impulsive total fields to fulfill the FFE.

4.2. Designing Virtual Experiments via FM

Expressions (21) and (22) suggest that one can design a virtual experiment such that the scattered field seem to emerge from the pivot point r_p by using the result of the FM equation. In doing so, the weighting function $w(\theta)$ defining the virtual experiment (see Eq. (5)) will not be directly the result of the qualitative preprocessing (i.e., the solution of the FM Equation (10)). In fact, for a given pivot point, the FM result has to be further processed by projecting it onto the singular system and then summing the projections according to Eq. (22).

In short, for each $\underline{r}_p \in \Omega$, the excitation distribution required to obtain a virtual scattered field that matches Ψ_∞ is given by the i_{FM} in Eq. (22), and the corresponding virtual incident field reads:

$$\Psi_{inc}(\underline{r},\underline{r}_p) = \int_\Gamma i_{FM}(\theta,\underline{r}_p)e^{-jk\hat{\theta}\cdot\underline{r}}ds(\theta), \tag{23}$$

wherein the dependence on the pivot point $\underline{r}_p$ has been explicitly highlighted.

As explained before, i_{FM} can be in principle unbounded. However, this circumstance is avoided in practice by using the regularized FM solution in Eq. (13) to cast the VE. This also allows to avoid instabilities arising from noise on data (which affects the SVD of $\mathcal{F}_m$). Hence, by replacing the regularized FM solution in Eq. (13) into Eq. (22), and taking into account the orthonormality of singular functions, we obtain the explicit expression of the primary source distribution underpinning FM designed VE, which reads:

$$i_{FM}(\theta, \underline{r}_p) = \sum_{n=0}^{\infty} \frac{1}{\xi_n + \alpha} \left\langle \Psi_\infty(\underline{r}_p, \varphi), \mu_n(\varphi) \right\rangle_\Gamma \mu_n(\theta). \tag{24}$$

By construction, such an excitation function is the one required to give raise to a virtual experiment in which the virtual far-field pattern matches $\Psi_\infty(\underline{r}_p, \varphi)$ on Γ.

5. LINEAR QUANTITATIVE INVERSION VIA FACTORIZATION METHOD DESIGNED VIRTUAL EXPERIMENTS

In the following, we show how to take advantage of FM in the linear inversion method proposed in [6].

Let us consider the pivot point $\underline{r}_p$, which defines a virtual experiment designed exploiting the FM as described above. In such an experiment, the exact (virtual) total field is given by:

$$\Psi_t(\underline{r}, \underline{r}_p) = \int_\Gamma i_{FM}(\theta, \underline{r}_p) E_t(\underline{r}, \theta) ds(\theta) = \Psi_{inc}(\underline{r}, \underline{r}_p) + \int_\Omega G(\underline{r}, \underline{r}') \Psi_t(\underline{r}', \underline{r}_p) \chi(\underline{r}') d\underline{r}'. \tag{25}$$

The second term at the right hand side is the virtual scattered field. Hence, by particularizing Eq. (25) for $\underline{R} \in \Gamma$, this last term is given by:

$$\Psi_s(\underline{R}, \underline{r}_p) = \int_\Gamma i_{FM}(\theta, \underline{r}_p) E_s(\underline{R}, \theta) ds(\theta). \tag{26}$$

By construction, this field approximates[†] the one radiated by an elementary source located in the pivot point. As such, it will be independent of the probed target. Conversely, the incident wave in Eq. (23) required to enforce this field depends on the scatterer under test through i_{FM}. Interestingly, this is the *opposite* of what happens in usual scattering experiments, where the scattered field (and the associated far-field pattern) change with the scatterer, while the incident field is independent from it.

The above suggests that exploiting the continuity of the field's tangential component, one can achieve an approximation for the field in the whole space by analytically continuing the scattered field from Γ to Ω. In particular, recalling that Ψ_∞ is the far-field pattern for the cylindrical wave radiated by an elementary source in $\underline{r}_p$, the virtual total field $\forall\ \underline{r} \neq \underline{r}_p$ can be approximated as:

$$\Psi_t(\underline{r}, \underline{r}_p) \approx \tilde{\Psi}_t(\underline{r}, \underline{r}_p) = \Psi_{inc}(\underline{r}, \underline{r}_p) - \frac{j}{4} H_0^2(k_b |\underline{r} - \underline{r}_p|), \tag{27}$$

wherein H_0^2 is the Hankel function of zero-th order and second kind. To avoid singularities, the value of the total field in $\underline{r}_p$ (if needed from a practical point of view) is obtained by averaging the nearby values or by exploiting the low pass filtering procedure described in [6].

By relying on such an approximation, the data-to-unknown relationship can be linearized as:

$$\Psi_s(\underline{R}, \underline{r}_p) = \int_\Omega G(\underline{R}, \underline{r}') \tilde{\Psi}_t(\underline{r}', \underline{r}_p) \chi(\underline{r}') d\underline{r}'. \tag{28}$$

By considering a collection of pivot points, $\underline{r}_1, \ldots, \underline{r}_P$, one can obtain a system of P linear integral equations (28), whose (regularized) inversion provides the estimate of the contrast. To select the pivot points, one relies on the estimated support given by the FM indicator. As discussed in [6], an even spacing of the pivot points within the estimated support is a convenient (and simple) choice. Their number can be either ruled by the number of incident fields (i.e., the original experiments) or by the degrees of freedom of the field radiated by a source having the same dimension as the estimated support.

[†] Within the level of accuracy of the regularized FM solution.

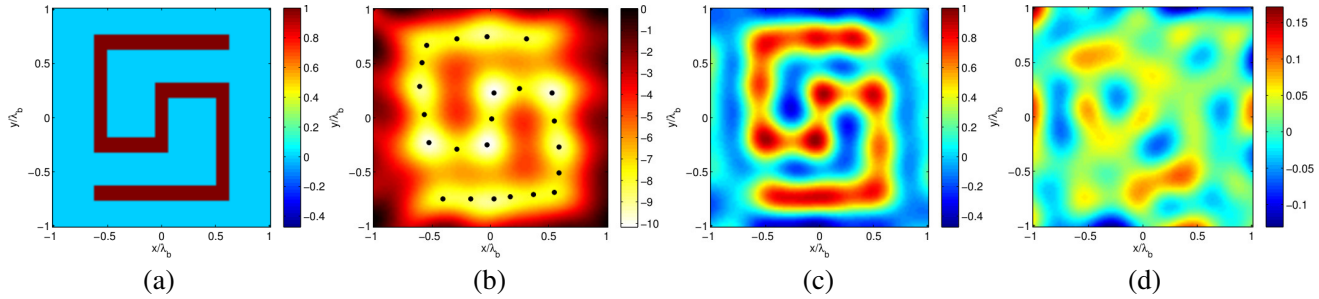

Figure 1. The *double-hook* shaped target. (a) Real part of the actual contrast; (b) estimated shape, with the selected pivot points superimposed; (c) real and (d) imaginary part of the retrieved contrast.

It is worth remarking that since the approximated virtual total field is tailored to the target (in an implicit fashion) via the FM preprocessing, the adopted linearization is deeply different from the Born approximation wherein the target is instead neglected. As such, the proposed approximation will have, by its nature, an extended validity range. On the other hand, the exploited approximation relies on the applicability of the FM, which entails for instance that multi-view multi-static data are required.

6. NUMERICAL EXAMPLES

In this section, we report some results of quantitative profiling achieved with the linearized inversion method described in the previous Section. The inversion result is achieved inverting the discretized counterpart of the system of P linear integral Eq. (28), regularized by means of the truncated singular value decomposition (TSVD) scheme, whose truncation index N_T is set by means of the Picard's plot method [6]. The reconstruction are quantitatively appraised using the normalized mean square distance between the actual and retrieved (complex) profiles, i.e., $err = \|\chi - \hat{\chi}\|^2/\|\chi\|^2$.

6.1. Synthetic Data: Double Hook Shaped Scatterer

The first example deals with the double-hook shaped lossless target shown in Fig. 1(a), whose relative dielectric permittivity is 2. The target is probed by means of $N = 18$ plane waves at 1 GHz, evenly spaced in angle, and the corresponding scattered fields are collected at $M = 18$ measurement points on a circle of radius 2λ. According to theoretical results [19], this number of probes is sufficient to collect, in a non-redundant fashion, all the available information in this experiment. The square imaging domain is large $2\lambda \times 2\lambda$, λ being the wavelength in homogeneous background medium (free space), and it is discretized into 100×100 cells to solve (via method of moments) the forward problem needed to simulate the data. These latter are corrupted with a SNR = 25 dB to simulate measurements errors.

The first step of the inversion procedure aims to recover the support of the scatterer. Fig. 1(b) shows the map of the FM indicator, i.e., the normalized logarithmic plot of $\|h\|$. This latter has been obtained by computing the SVD of the $M \times N$ data matrix and setting $\alpha = 0.2$ in (13). On the basis of such an image, we select $P = 23$ evenly spaced pivot points, marked as black dots in Fig. 1(b). Note we have taken a number of pivot points slightly larger than N, in order to cover the estimated support with almost evenly spaced pivot points. The quantitative reconstruction, achieved for a truncation index $N_T = 71$, is shown in Figs. 1(c), (d). As we can see, both shape and electric properties of the scatterer are fairly recovered, the reconstruction error being as low as $err = 0.42$.

6.2. Assessment against Experimental Fresnel Benchmark Data

To further test the use of FM designed virtual experiments for quantitative inversion purposes, we have processed some experimental data provided by the Fresnel Institute of Marseille, France. For details on these datasets, we address the reader to [13, 14], while below we recall the difficulties to face when dealing with them.

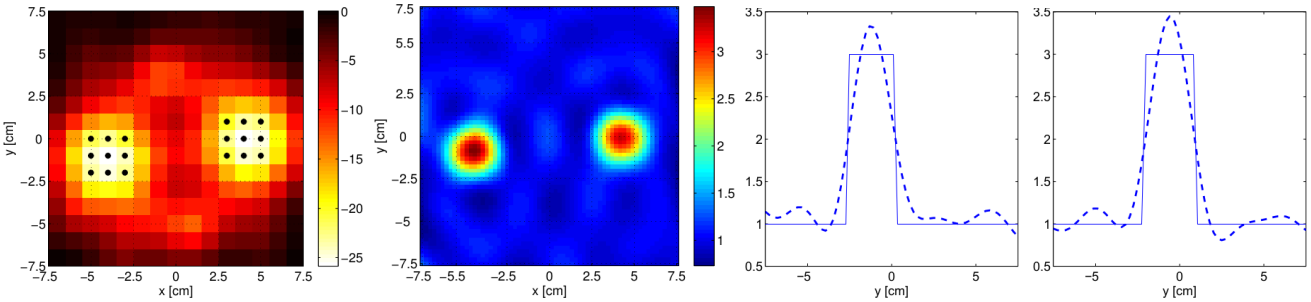

Figure 2. TwodielTM Fresnel dataset at 4 GHz. (a) Normalized logarithmic plot of the FM indicator. A coarse grid (15×15) is used to allow selecting in an automatic way the pivot points for the VE; (b) Map of the retrieved dielectric permittivity over a 64×64 grid. Central cut of the retrieved permittivity profile along the y axis: (c) leftmost cylinder; (d) rightmost cylinder.

The first difficulty to face when dealing with the Fresnel dataset is that these experiments have been carried under a partially aspect limited measurement configuration to which FM cannot be straightforwardly applied. In particular, the illuminations completely surround the targets, but, for each illumination, measurements are taken only on a 240° arc, i.e., by excluding a 120° arc centered on the emitter. Hence, to apply the FM as design equation, we have simply filled with zeros the measurement entries not available in the data matrix and computed Ψ_∞ for all the measurement positions considered over the circumference.

The second difficulty is the need of the incident field in the imaging domain to build the approximated virtual total field Ψ_t (25). To this end, we have adopted the approach in [21] and modeled the incident fields by means of a multipoles expansion, whose coefficients have been set via least square fitting of the incident field values measured at the receivers. Taking into account the dimension of the antenna's aperture ($0.143 \times 0.2413\,\mathrm{m}^2$), the number of multipoles is set, according to the working frequencies, as $2ka + 1$, with a being the radius of the antenna's surface $a = \sqrt{(0.143 \times 0.2413)/\pi}$.

6.2.1. TwodielTM Dataset: Two Homogeneous Dielectric Cylinders

The two identical dielectric cylinders (radius 1.5 cm, relative permittivity 3 ± 0.3) are spaced of about 5 cm [13]. For this dataset, $M = 49$ and $N = 36$, so that after the zero-filling procedure, we obtain $M' = 72$ measurement positions and processed a 72×49 data matrix. The result of the qualitative processing of the 4 GHz frequency data is shown in Fig. 2(a). To the best of our knowledge, this is the first time FM is applied to the Fresnel dataset and it is worth noting that, thanks to the adopted data organization strategy, the FM succeeds in retrieving the features of the targets. The value of the Tickhonov parameter in FM has been set as $\alpha = 9.1\times10^{-3}$. Such qualitative inversion has been run on a coarse grid to perform an almost automated (and fast) selection of the pivot points. As a matter of fact, we can simply pick as pivot points all the sampling points where the indicator is above -20 dB, which approximately outline the estimated support. In this respect, it is worth noting that the exact boundary of the scatterer is not strictly required by the method, which only needs to accommodate a sufficient number of (almost evenly spaced) pivot points within the estimated support. Finally, the obtained VE are used to cast the linearized inversion, which leads to the reconstruction shown in Figs. 2(b)–(d), with $N_T = 77$. As can be seen, the value of the permittivity, as well as the positions, the shapes and the dimensions of the two targets, are correctly retrieved. The reconstruction error with respect to a simulated profile having the one declared for this target in [13] is 0.4.

6.2.2. FoamDielIntTM Dataset: Two Nested Cylinders

This dataset consists of two nested cylinders. The inner one has radius 1.5 cm and relative permittivity 3 ± 0.3, while the outer cylinder has 4 cm and relative permittivity 1.45. The two cylinders are almost

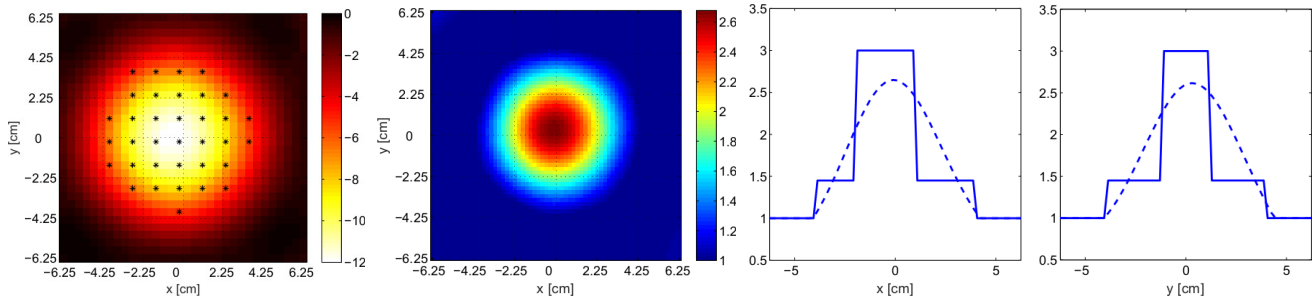

Figure 3. FoamDielIntTM Fresnel dataset at 2 GHz. (a) Normalized logarithmic plot of the FM indicator. A coarse grid (32×32) is used for automated pivot points selection; (b) Retrieved dielectric permittivity over a 64×64 grid. To better visualize the reconstruction, we have forced to zero the pixels without physical meaning for a vacuum background, i.e., those wherein the retrieved relative permittivity is lower than one. Central cut of the retrieved permittivity along the (c) x and (d) y axis.

co-centric. For this dataset, $M = 241$ and $N = 8$. At the considered frequency of 2 GHz, this number of measurements is exceedingly large [19]. Hence, we have first filled with zeroes the missing measurement positions and then undersampled the data to $M' = 72$ measures on the whole circumference (part of them are forced to be zeroes). Finally, we have computed the FM indicator for a 72×8 data matrix, assuming a Tickhonov parameter $\alpha = 0.0082$. The result of the qualitative processing of the data at 2 GHz is shown in Fig. 3(a). Also in this case, the qualitative inversion has been run on a coarse grid (32×32) to allow an automated selection of the (35) pivot points, see Fig. 3(a). The resulting VE are used to cast the linearized inversion with $N_T = 17$. The reconstruction is shown in Fig. 3(b), and corresponds to an error as low as 0.29. Notably, this is the first time in which the VE based linear inversion scheme is applied to Fresnel inhomogeneous targets. As can be seen the value of the permittivity, as well as position, shape and non homogeneous nature of the targets, can be easily inferred from Figs. 3(b)–(d), but for a slight underestimation of the inner cylinder, which is, to some extent, complementary to the overestimation experienced in the $TwoDielTM$ dataset.

To conclude this assessment, let us discuss the performance of the linear VE based inversion with respect to other methods that have been applied to the Fresnel targets, see for instance [13, 14], where the data were first presented. The first important comment is that the VE based method is the only one that, to the best of our knowledge, allows to achieve a quantitative image of such targets by using a linear inversion tool, rather than a non-linear iterative optimization, with obvious advantages in terms of robustness, reliability and computational effectiveness. In addition, our result has been achieved by using just a single frequency, whereas Fresnel targets are usually processed using multiple frequencies (either simultaneously or within a hopping procedure) [13, 14]. On the other hand, since our method is not enforcing any kind of edge preserving regularization, but rather pursues the "minimum-energy" solution, the achieved reconstruction does not allow to fully appreciate the piece-wise homogeneous nature of the targets. Such an issue could be overcome using the sparsity enhanced VE approach in [10], but this would entail an increase in terms of computational complexity, which is instead negligible in the case at hand.

The choice of the frequency is obviously an important point, as it affects the performance of FM and henceforth the accuracy of the VE. In particular, it is well known that sampling methods like FM properly work when the targets are in the resonant region (i.e., are comparable to the probing wavelength) [15, 18]. Accordingly, given the assumed size of the imaging region, we have selected those frequencies for which the whole region has an electric dimension comparable to the wavelength. Another important aspect is to ensure that a sufficient number of incident fields and/or measurement directions is available. The criterion adopted to verify this conditions is to ensure a number of incident fields in the order of the degrees of freedom of the region under test [19].

Finally, it is worth noting that the adopted approximation has a larger validity than the Born approximation, both in terms of permittivity values and electrical dimensions of the targets. While,

for the sake of brevity, herein we do not report comparisons, we address the reader to [7, 9, 24] for a comprehensive performance assessment of these two linearized inversion methods.

7. CONCLUSIONS

We have shown that the factorization method can be used as a tool to design virtual scattering experiments. In particular, exploiting the properties of the relevant operator, a convenient rewriting of the FM equation has been derived to elucidate the relationship between the FM operator and the physical quantities involved in the underlying scattering experiments. This rewriting also allows a physical interpretation of FM in terms of spatial focusing, thanks to the apparent analogy with the LSM equation.

The VE designed via FM, anchored to the solid mathematical background behind this method, can be exploited in a number of methods based on this novel paradigm, de facto extending the capabilities of this FM from qualitative to quantitative imaging. Notably this class of new methods is deeply different from the so-called hybrid methods [22, 23], which pair a qualitative inversion and a quantitative reconstruction in cascade, using the qualitative step "only" to estimate the targets' support. Conversely, in VE-based methods, the information arising from the qualitative step is exploited not only to estimate the support, but also, and more important, to condition the behavior of the internal field, which is unknown in the diffraction tomographic imaging. As an example, we have shown some results with a linearized inversion method [6] that allows to perform quantitative reconstructions of dielectric targets far beyond the validity range of the Born approximation, thanks to an effective, target driven, approximation of the virtual total field which exploits the processing of the data via FM.

As a final comment, it is worth pointing out that the VE method is deeply different from the unrelated illuminations method [25, 26]. As a matter of fact, while both methods exploit field focusing, the unrelated illuminations method pursues the focusing of the *incident* fields (in the imaging domain), rather than the focusing of the *total* fields (in the scatterers' support). Besides this (significant) difference, it is worth noting that the unrelated illuminations method claims to achieve the contrast by focusing the incident fields in each pixel of the scenario and solving the resulting local (direct) inversion. However, such a claim ignores the fact that incident fields have a finite number of degrees of freedom [19], so that it is not possible to shape them at will, unless unbounded energy excitations are used. Since finite energy primary source must be used in practice, it turns out that the unrelated illuminations method is not viable in any practical situation.

REFERENCES

1. Colton, D. and R. Kress, *Inverse Acoustic and Electromagnetic Scattering Theory*, Springer-Verlag, Berlin, Germany, 1992.
2. Cakoni, F. and D. Colton, *Qualitative Methods in Inverse Scattering Theory*, Springer-Verlag, Berlin, Germany, 2006.
3. Potthast, R., "A survey on sampling and probe methods for inverse problems," *Inv. Probl.*, Vol. 22, R1–R47, 2006.
4. Colton, D. and A. Kirsch, "A simple method for solving inverse scattering problems in the resonance region," *Inv. Probl.*, Vol. 12, 383–393, 1996.
5. Kirsch, A. and N. I. Grinberg, *The Factorization Method for Inverse Problems*, Cambridge, 2008.
6. Crocco, L., I. Catapano, L. Di Donato, and T. Isernia, "The linear sampling method as a way to quantitative inverse scattering," *IEEE Trans. Antennas Propagat.*, Vol. 60, No. 4, 1844–1853, Apr. 2012.
7. Di Donato, L. and L. Crocco, "Model-based quantitative cross-borehole GPR imaging via virtual experiments," *IEEE Trans. Geosci. Remote Sens.*, Vol. 53, No. 8, 4178–4185, Aug. 2015.
8. Bevacqua, M. T., L. Crocco, L. Di Donato, and T. Isernia, "An algebraic solution method for nonlinear inverse scattering," *IEEE Trans. Antennas Propagat.*, Vol. 63, No. 2, 601–610, Feb. 2015.

9. Di Donato, L., M. T. Bevacqua, L. Crocco, and T. Isernia, "Inverse scattering via virtual experiments and contrast source regularization," *IEEE Trans. Antennas Propagat.*, Vol. 63, No. 4, 1669–1677, Apr. 2015.
10. Bevacqua, M. T., L. Crocco, L. Di Donato, and T. Isernia, "Microwave imaging of nonweak targets via compressive sensing and virtual experiments," *IEEE Antennas Wireless Propagat. Lett.*, Vol. 14, 1035–1038, 2015.
11. Di Donato, L., R. Palmeri, G. Sorbello, T. Isernia, and L. Crocco, "A new linear distorted-wave inversion method for microwave imaging via virtual experiments," *IEEE Trans. Microwave Th. Tech.*, Vol. 64, 2478–2488, 2016.
12. Arens, T., "Why linear sampling works," *Inv. Probl.*, Vol. 20, 163–173, 2004.
13. Belkebir, K. and M. Saillard, "Guest editors' introduction," *Inv. Probl.*, Vol. 17, 1565, 2001.
14. Belkebir, K. and M. Saillard, "Testing inversion algorithms against experimental data: Inhomogeneous targets," *Inv. Probl.*, Vol. 21, S1, 2005.
15. Crocco, L., L. Di Donato, I. Catapano, and T. Isernia, "An improved simple method for imaging the shape of complex targets," *IEEE Trans. Antennas Propagat.*, Vol. 61, No. 2, 843–851, 2013.
16. Hanson, G. W. and A. B. Yakovlev, *Operator Theory for Electromagnetics*, Springer-Verlag, NY, 2002.
17. Bertero, M. and P. Boccacci, *Introduction to Inverse Problems in Imaging*, Institute of Physics, Bristol, UK, 1998.
18. Catapano, I., L. Crocco, and T. Isernia, "On simple methods for shape reconstruction of unknown scatterers," *IEEE Trans. Antennas Propagat.*, Vol. 55, 1431–1436, 2007.
19. Bucci, O. M. and T. Isernia, "Electromagnetic inverse scattering: Retrievable information and measurement strategies," *Radio Sci.*, Vol. 32, 2123–2138, 1997.
20. Cabayan, H. S. and G. A. Deschamps, "Antenna synthesis and solution of inverse problems by regularization methods," *IEEE Trans. Antennas Propagat.*, Vol. 20, No. 3, 1972.
21. Crocco, L. and T. Isernia, "Inverse scattering with real data: Detecting and imaging homogeneous dielectric objects," *Inv. Probl.*, Vol. 17, No. 6, 1573, 2001.
22. Catapano, I., L. Crocco, M. D'Urso, and T. Isernia, "On the effect of support estimation and of a new model in 2D inverse scattering problems," *IEEE Trans. Antennas Propagat.*, Vol. 55, 895–1899, 2007.
23. Brignone, M., G. Bozza, A. Randazzo, M. Piana, and M. Pastorino, "A hybrid approach to 3D microwave imaging by using linear sampling and ACO," *IEEE Trans. Antennas Propagat.*, Vol. 56, 3224–3232, 2007.
24. Di Donato, L., R. Palmeri, G. Sorbello, T. Isernia, and L. Crocco, "Assessing the capabilities of a new linear inversion method for quantitative microwave imaging," *Int. J. Antenn. Propag.*, Vol. 2015, 9 pages, ID 403760, 2015.
25. Wang, W. and S. Zhang, "Unrelated illumination method for electromagnetic inverse scattering of inhomogeneous lossy dielectric bodies," *IEEE Trans. Antennas Propagat.*, Vol. 40, 1292–1296, 1992.
26. El-Babli, I. and A. Sebak, "Unrelated illumination approach for the reconstruction of three dimensional inhomogeneous dielectric bodies," *Journal of Electromagnetic Waves and Applications*, Vol. 12, 371–385, 1998.